

Coherent temperature-wave generation in SrTiO_3 by stimulated light-scattering

Akitoshi Koreeda, Hideaki Oe, Takahiro Okada, and Yasuhiro Fujii¹

¹*Department of Physical Sciences, Ritsumeikan University, Kusatsu, 525-8577, Shiga, Japan*

(Dated: December 8, 2022)

Wave propagation of heat in solids, which is often referred to as “second sound”, has been attracting increasing attention in relation to various potential applications such as thermal diodes, waveguides, and so on. Until recently, second sound had been just a subject of observation because it is very rarely realised in solids. It has been suggested that ferroelectrics are strong candidates for thermal-wave media¹, and several reports on an incipient ferroelectric, strontium titanate (SrTiO_3), showed a novel wave-like excitation in light-scattering spectra^{2,3}, and second sound has been proposed for the most plausible origin for this excitation based on rather indirect demonstration^{3,4}. However, the lack of a direct demonstration still leaves controversy⁵ on the existence of second sound in SrTiO_3 . Here we show a direct demonstration of the optically-generated coherent wave of heat, i.e., coherent second sound, in bulk single crystals of SrTiO_3 . The generated wave-excitation has a linear dispersion relation with a predicted velocity of second sound in this material, and is overdamped at high temperatures or low frequencies, exhibiting apparently diffusive behaviour with the decay rates defined by the known values of the thermal diffusivity of SrTiO_3 . This work offers not only convincing evidence for the existence of second sound in SrTiO_3 , but also a first demonstration of coherent generation and wave-control of gigahertz temperature fields in a 3D bulk material. As high-quality SrTiO_3 is widely available, and it is also known as a mother material of superconductors, the coherent excitation of temperature wave in this material offers a pathway for potential novel wave-based applications in heat management such as construction of thermal waveguides and directional devices, or heat-control of superconductivity.

Thermal transport in insulators is realised by lattice vibrations, or in other words, by phonons, which are quantised sound waves. Recently, phonon-related physics has been attracting much attention, such as phonon Hall effect⁶, phonon spin/orbital angular momenta^{7,8}, and phonon hydrodynamics⁹. Hydrodynamic phonon excitation allows for wave propagation of the collection of phonons, that is, wave propagation of temperature field in solids. Such a wave excitation of temperature is referred to as “second sound”, named after its slower propagation speed than ordinary (first) sound, although second sound is not a sound. Second sound is a very rare phenomenon, and only limited numbers of materials have been reported as candidates for its medium^{3,5,10–13}, so far. Among these materials, strontium titanate (SrTiO_3) has had a long-standing controversy on the existence of second-sound excitation^{2,3,5,14–20}.

SrTiO_3 is one of the most popular materials, which are widely used in researches and industry as a diamond simulant, substrates for perovskite-crystal growth, and so on. It is well-known that SrTiO_3 , which is an insulator without doping, becomes metallic by slight doping of Nb ions, and that it becomes even a superconductor²¹, which has been attracting much interest even today. Also, phonon-related interesting phenomena in SrTiO_3 including Poiseuille flow of hydrodynamic phonons⁴ and phonon hall effect⁶ are suggested recently. SrTiO_3 is known as a quantum paraelectric, which does not undergo ferroelectric phase transition due to the relatively large quantum fluctuations of a polar lattice vibration, so-called ferroelectric “soft mode”²². This situation is advantageous for the existence of second sound because the low-frequency and long-wavelength soft mode is thermally excited even at cryogenic temperatures¹.

Experimentally, second sound in SrTiO_3 was first suggested by Hehlen et al² according to the anomalous Brillouin light scattering spectrum. After 12-year controversy^{14–17}, Ko-

reeda et al^{3,18} reported that second sound is likely to exist in SrTiO_3 from the analysis of the Brillouin spectra based on extended irreversible thermodynamics²³. However, as the line-shape analysis was rather complicated, the existence of second sound in SrTiO_3 has still been stated to be very unlikely^{17,19}, or controversial⁵, or limited to an indirect demonstration⁹. For facilitating future applications of three dimensional novel thermal devices such as diodes or waveguides of heat, convincing demonstration that SrTiO_3 is a medium of propagating second sound has long been awaited.

In this Article, we demonstrate the optical generation of coherent wave of temperature field in SrTiO_3 . This is the first “direct” demonstration of the second-sound propagation in this material, providing convincing evidence for settling the long standing controversy^{2,3,5,14–20}. By systematically changing the wavelength and frequency of the excitation generated in our transient-grating method²⁴, we find that the generated wave excitation has a predicted velocity of second sound in SrTiO_3 . We show that the generated wave excitation is overdamped at long wavelengths and low frequencies, while at high temperatures, it transforms into apparent diffusive behaviour, with a predicted decay rate of thermal diffusion in this material. Combining our data with those reported in low-frequency light scattering experiments at much shorter wavelengths^{3,18,25}, we show that both the normal (momentum-conserving) and resistive (momentum-destroying) phonon-scattering rates can be easily obtained from quite a simple analysis of the wavenumber dependences of the frequency and damping rate of second sound. The obtained phonon-scattering rates are in excellent agreement with the previously reported values^{3,18}, firmly verifying that the second-sound window is widely open, i.e., the normal scattering is much more frequent than the resistive scattering in cryogenic SrTiO_3 .

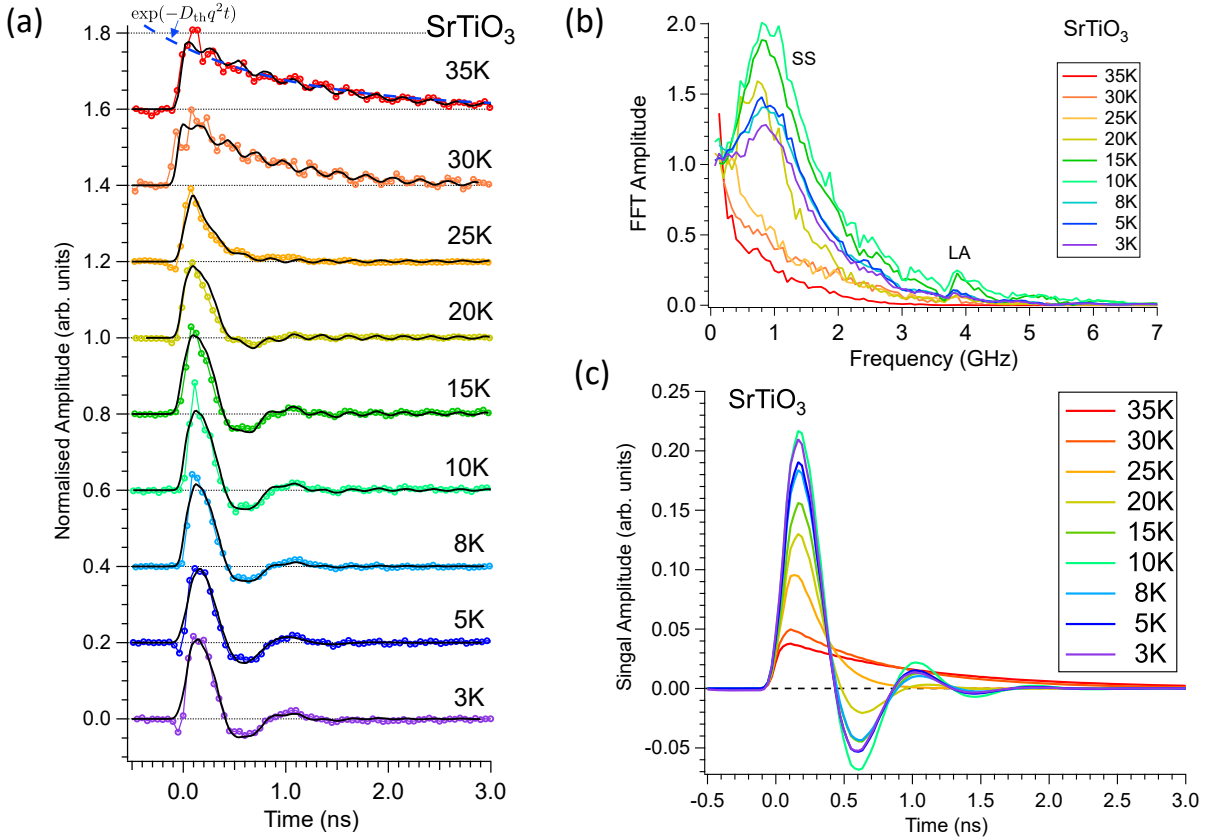


FIG. 1. (a) Temperature variation of the temporal profiles observed in SrTiO_3 . All traces were obtained after smoothing and subtraction of the residual constant offset due to the electronic excited state (see Extended Data Fig. 3). (b) Fourier-transformed spectra of the observed temporal signals. SS and LA denote second sound and longitudinal acoustic phonon, respectively. (c) Temperature variation of the large, slow oscillation extracted by fitting Eq. (1) to the temporal profiles.

FROM THERMAL DIFFUSION TO THERMAL WAVE

The samples of SrTiO_3 were synthesised single crystals. We used two samples: Sample A and B. Sample A, which is very slightly amber coloured, was purchased in 1995 and it is identical with that employed in previous studies^{3,18,26}. Sample B was purchased in 2022, which was non-coloured and transparent. Both Samples A and B were blocks with dimensions of $10 \times 8 \times 7 \text{ mm}^3$, with surfaces oriented to $[001]$, $[110]$, and $[1\bar{1}0]$ in the cubic phase. The transient grating was formed along crystalline $[001]$ direction in the cubic phase, i.e., the wavevector \mathbf{q} was set parallel to $[001]_c$. Other direction of \mathbf{q} turned out to provide stronger damping, probably due to the anisotropy of the thermal conductivity in the tetragonal phase of SrTiO_3 .

Figure 1a shows the temperature variation of the temporal profiles, which were obtained by optically-heterodyne-detected thermal grating technique²⁴ with a grating wavenumber of $2.8 \times 10^6 \text{ rad/m}$ (a grating period of $2.2 \times 10^{-6} \text{ m}$), after subtraction of backgrounds (see Extended Data Figs 1, 2, 3). The weak oscillation appearing on all the traces is due to the longitudinal acoustic (LA) phonon mode, which was identified from the known LA-sound velocity ($v_{\text{LA}} \approx 8.0 \times 10^3 \text{ m/s}$)

and employed wavenumber q according to the dispersion relation $f = v_{\text{LA}}q/2\pi = 3.6 \times 10^9 \text{ Hz}$.

Our subject is the much more dominant component in the traces. The traces at relatively high temperatures in Fig. 1a appear to be exponential decays, which are identified to be the thermal-diffusion signal as reported in Ref.26. Indeed, we could overlay $\exp(-D_{\text{th}}q^2t)$ on the 35 K data with the reported value of the thermal diffusivity $D_{\text{th}} = 6.0 \times 10^{-5} \text{ m}^2/\text{s}$ for both Samples A and B, which is indicated by the blue dashed curve on the 35 K trace in Fig. 1a. At relatively low temperatures, we see that the thermal-diffusive signal transforms into underdamped oscillation with a period of approximately 0.8 ns. Figure 1b displays the spectra calculated by fast Fourier transform (FFT) of the temporal profiles shown in Fig 1a. The large oscillatory component yields a resonance peak at around 1 GHz, while it vanishes at high temperatures above 20 K. The weak peak at around 3.8 GHz corresponds to the LA-phonon resonance, which has an asymmetric “Fano-type” lineshape similar to those observed in spontaneous Brillouin scattering^{2,3,26}.

Both Figs. 1a, 1b, and 1c are just like what are found in most textbooks on classical mechanics: it is quite well-known as temporal and frequency dependences of the amplitude of

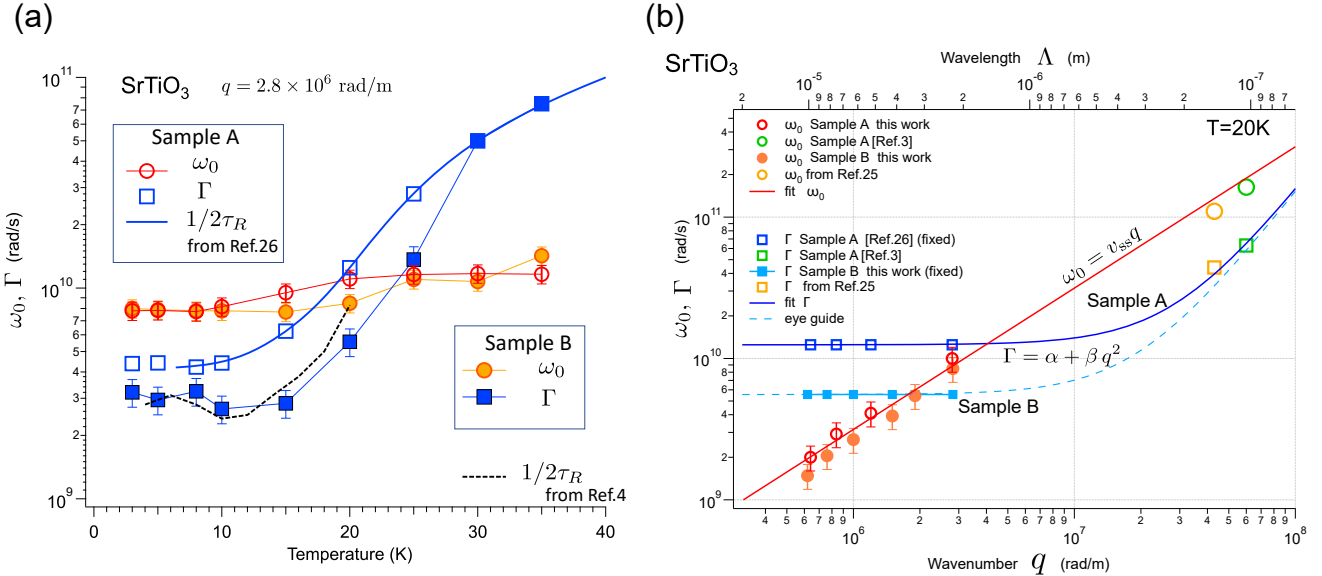


FIG. 2. (a) Temperature dependences of the natural angular frequency (ω_0) and damping rate (Γ) in Samples A and B. The literature values of $1/2\tau_R$ cited from Refs. 26 and 4 are also displayed. (b) Wavevector dependences of ω_0 and Γ in Samples A and B (log-log plot). The points at large q -values are cited from Refs. 3 and 25. The red straight line and the blue curve are a fit to ω_0 - and Γ -values obtained in Sample A, respectively. The dashed curve is a guide to the eye for Γ in Sample B: it is drawn using $\alpha = 5.6 \times 10^9 \text{ rad/g}$ and the same value of β obtained for Sample A.

a damped-harmonic-oscillator, when it is rest at the equilibrium position and impulsively excited with a finite initial velocity given by a hammer impact. In our experimental condition, the temperature rise relevant for the formation of the thermal grating is virtually impulsively produced by fast non-radiative relaxations (typically $\sim \text{ps}$ order) of the two-photon absorbed energy given by the picosecond pulsed-laser irradiation of 532 nm wavelength^{26,27}.

Each of the temporal profiles was successfully fitted by a damped harmonic oscillator (DHO) function as

$$S(t) \propto \frac{\omega_0}{\Omega} e^{-\Gamma t} \sin \Omega t, \quad \Omega \equiv \sqrt{\omega_0^2 - \Gamma^2}, \quad (1)$$

plus a weak LA-phonon oscillation (for details of analysis, see Methods and Extended Data Fig. 3). ω_0 and Γ are the natural angular frequency and damping rate of the DHO, respectively. The fitted functions are overlaid on the experimental points in Fig. 1a as black curves. Figure 1c displays the extracted response corresponding to the dominant component expressed by Eq. (1). Since we have already identified that the high-temperature traces are due to thermal diffusion, which is “overdamped thermal wave”, the oscillating signals must be interpreted as arising from underdamped wave propagation of heat, i.e., second sound.

DISCUSSION

We show in Fig. 2a the temperature dependences of the natural angular frequency ω_0 obtained by function fitting of

Eq. (1) to the observed temporal profiles as well as the values of Γ employed in our analysis. The fact that thermal diffusion is observed in our experiments allows us to assume that hydrodynamic-phonon regime¹⁸ is realised in our experimental condition. Thus, we may assume that the damping rate of the thermal wave for small wavenumbers to be $\Gamma \approx 1/2\tau_R = \bar{v}_{\text{ph}}^2/6D_{\text{th}}$ ¹⁸, where τ_R is the resistive phonon scattering time, and \bar{v}_{ph} is the averaged phonon velocity. Since Sample A is exactly the same specimen employed in the study of Ref. 26, we can use the (interpolated) value of D_{th} reported in Ref. 26 at all the temperatures investigated in the present study, except 3 K and 5 K. With the Γ -value fixed in the DHO-function fitting at each temperature, the values of ω_0 were successfully determined with minimum uncertainty in Sample A. For Sample B, we could employ the same Γ -values with Sample A only for 30 K and 35 K. For lower temperatures, however, Sample B exhibited more weakly damped oscillations than Sample A, and we could find appropriate values for Γ , by assuming a weak and smooth temperature dependence of ω_0 like that found in Sample A. In fact, the underdamped signals (decaying oscillations) can be successfully fitted with both ω_0 and Γ being independent free parameters, because the temporal shape contains independent information of ω_0 and Γ , which are relevant for the oscillation period and decaying rate, respectively. We also plotted in Fig. 2a the values of $1/2\tau_R$ calculated from the values of mean free path reported by Martelli et al⁴, showing good agreement with Γ obtained in Sample B at $T \lesssim 20 \text{ K}$.

We see in Fig. 2a that $T \approx 18 \text{ K}$ and $T \approx 23 \text{ K}$ are the critical temperatures between overdamping (thermal diffusion) and underdamping (thermal wave) in Sample A and

B, respectively, for the employed value of q . We obtained relatively small values of Γ in Sample B compared to those in Sample A. This is probably due to the sample quality such as concentration of the oxygen vacancies or impurities. On the other hand, we obtained similar values of ω_0 in both samples. This is because ω_0 is basically associated with the average phonon velocity or the speed of second sound (described below), which is determined solely by the phonon dispersion relation (common to both samples) rather than the scattering rate of phonons.

If the generated oscillation is due to a wave, the frequency ω_0 and wavenumber q must obey the dispersion relation as $\omega_0 = qv$, where v is the phase velocity of the wave. It is known that second sound has a velocity given by $v_{ss} \approx \frac{1}{\sqrt{3}}\bar{v}_{ph}$. With the known value of $\bar{v}_{ph} \approx 5.4 \times 10^3$ m/s (from Debye's model) for SrTiO₃, we estimate that $v_{ss} \approx 3.1 \times 10^3$ m/s. We also investigated the wavenumber (q) dependence of the generated excitation (see Extended data Fig.4). Since we investigated the q -dependence at a fixed temperature, viz., $T = 20$ K, Γ was fixed in the analysis of q -dependence. We set the Γ -value to be 1.3×10^9 rad/s and $\Gamma = 5.6 \times 10^9$ rad/s for Samples A and B, respectively, as shown in Fig. 2a. Regardless of employing this q -independent Γ , each of the temporal profiles observed at various q -values was quite successfully fitted again by a DHO function of Eq. (1) plus weak LA-phonon oscillation (see Extended data Fig.4).

Figure 2b shows the q -dependence of ω_0 measured at 20 K in Samples A and B, as well as the values reported in the spectral analyses for the broad Brillouin-scattered peak measured at ≈ 20 K presented in Refs. 3 and 28. We clearly see that $\omega_0 \propto q$, i.e., a linear dispersion relation, indicating that the oscillation arises from a wave excitation of wavelengths $\Lambda = 2\pi/q$, and the slope of the plots gives the propagation velocity of the wave. Furthermore, the points cited from Refs. 3 and 28 are located on a common line with the points obtained in this work, indicating that the generated wave-excitation has the same physical origin with the broad Brillouin-scattered peak. From a line fitting to all of the ω_0 -values against q for Sample A including the data for much larger wavenumbers ($q = 4.2 \times 10^7$ [Ref.28], and 6.0×10^7 rad/m [Ref.3]), the velocity of the wave was found to be $\approx 3.1 \times 10^3$ m/s, which is in excellent agreement with the predicted second-sound velocity. We also plot the values of the damping rates Γ in Fig. 2b. Since Γ is constant at small q -values, the magnitudes of ω_0 and Γ cross at around a “critical wavenumber” of $q_c \approx 4.0 \times 10^6$ and 2.0×10^6 rad/m for Samples A and B, respectively, i.e., $\omega_0 > \Gamma$ for $q > q_c$, and vice versa. We observed that the generated signal became “diffusive” when $q \ll q_c$, and oscillatory when $q > q_c$ (see Extended Data Fig.4). This behaviour is quite simply understood that the generated thermal wave can exist as a weakly damped (underdamped) wave if $\omega_0 > \Gamma$ is satisfied.

For Γ at larger values of q , we again cite the published data based on the spectral analyses in the spontaneous Brillouin scattering studies^{3,28}. For the damping rate Γ in Sample A, the q -dependence is quite reasonably fitted by the predicted

relation for second sound as¹⁸

$$\Gamma = \alpha + \beta q^2, \quad \alpha = \frac{1}{2\tau_R}, \quad \beta = \frac{2}{5}v_{ss}^2\tau_N \quad (2)$$

where τ_R and τ_N are the resistive and normal scattering times of the phonons, respectively. With a fixed value of α , fitting of such a simple parabola as Eq. (2) to the q -dependence of Γ directly provides us the values of τ_N , with the knowledge of the second-sound velocity $v_{ss} = 3.1 \times 10^3$ m/s, which was just obtained from the dispersion relation, $\omega_0 = v_{ss}q$. For Sample A, the constant α was fixed to 1.3×10^{10} rad/s according to the separately measured value of $\tau_R = 3D_{th}/\bar{v}_{ph}^2 = 40$ ps for Sample A²⁶, and we could fit the blue curve in Fig. 2b to obtain $\beta = 1.5 \times 10^{-5}$ m²/s²rad, yielding $\tau_N = 3.9$ ps, which is in fair agreement with the previously reported value (≈ 5 ps) on SrTiO₃ at 20 K^{3,18}, and we see that the frequency window required for the existence of second sound²⁹ is open in Sample A. For Sample B, we may assume that τ_N takes similar value with Sample A, because τ_N should not be affected by sample quality as τ_R does, and is determined essentially by the frequency of the transverse optic phonon mode (soft mode)¹. We draw in Fig. 2b an eye-guide curve (the dashed curve) employing the same β -value as in Sample A. Since Γ in Sample B is about half the magnitude compared to Γ of Sample A, we estimate $\tau_R \approx 90$ ps. Thus, the frequency window for second-sound propagation is even more widely open in a newer crystal of SrTiO₃ like Sample B.

In terms of length scale, the mean free paths of normal and resistive phonons ($\bar{v}_{ph}\tau_N$ and $\bar{v}_{ph}\tau_R$, respectively) in Sample B at 20 K are estimated to be 21 nm and 490 nm, respectively, indicating that second sound having wavelengths between these values can propagate as a wave. As the reported size of the anti-ferrodistortive domains arising from the cubic-to-tetragonal structural phase transition at 105 K in SrTiO₃ is μm scale³⁰, the second sound propagating along [001]_c direction in cryogenic SrTiO₃ does not suffer much from domain wall scattering of phonons. Here, it is worth noting that we have directly obtained the value of τ_N just by fitting of quite a simple parabola function, instead of employing a complicated fitting function like one presented in Refs.3 and 18.

The q -dependence of the damping rate Γ presented above is a prominent feature and direct evidence of second sound. Although acoustic phonons are the only alternative candidate for the generated wave in this frequency range, they must have damping rate like $\Gamma_{ph} \propto q^p$, where the exponent p approaches 2 for small q and high T (Akhieser limit), and approaches 1 for large q and low T (Landau-Rumer limit)³¹. Therefore, the observed q -independence for small q -values and steeper q -dependence for large q -values is not compatible with the scenario of the attenuation of an acoustic-phonon mode²⁰.

The temperature and wavevector dependences shown in Figs. 2a and b allow us to unambiguously confirm that the generated wave excitation is the “coherent second sound” in SrTiO₃. Thus, we have succeeded in coherent generation of the temperature wave with well-defined and controllable frequency and phase. At the same time, the 27 year controversy^{2,3,5,14-20} over the broad Brillouin-scattered peak has been resolved, and it has been firmly identified as the spec-

trum of the “thermally excited” second sound in SrTiO_3 . Indeed, the FFT spectra shown in Fig. 1b and Extended data Fig.4 exhibit qualitatively the same lineshape as those reported in spontaneous Brillouin scattering experiments^{2,3,18}.

I. SUMMARY AND OUTLOOK

We have succeeded in generating coherent thermal wave (second sound) by stimulated Brillouin scattering technique in SrTiO_3 . We emphasise the difference between the “observation” of the thermally-excited second sound and the “generation” of coherent second sound. Whereas the broad Brillouin peak arises from the thermally-excited, “incoherent” ripples of temperature fluctuations with extremely small amplitudes, laser-pulse-induced stimulated scattering process actively generates “coherent” (in-phase) oscillations of temperature with much larger amplitudes. Our experimental achievement may open the way of controlling such eigenstates of heat. For example, we may be able to make various initial patterns of temperature rise by changing the figures displayed on the spatial light modulator employed in our apparatus (see

Methods and Extended Data Fig.1).

Although there is no experimental data so far in the q -value range from 1×10^7 to $\sim 3 \times 10^7$ rad/m, we find that the ratio ω_0/Γ is the largest for this q range. In fact, ω_0/Γ is expected to reach its maximum of ≈ 6 at $q = \sqrt{\alpha/\beta} \approx 1.8 \times 10^7$ rad/m, which corresponds to a second-sound wavelength of $\Lambda = 2\pi/q \approx 350$ nm. At this wavelength, the second-sound resonance in SrTiO_3 is expected to be the sharpest. Such a well-defined wave excitation would be sufficient for various kinds of wave-control of heat. Since SrTiO_3 is a 3D bulk crystal, wave-controlling elements such as reflecting interfaces (mirrors), lenses, or waveguides, seem to be easily constructed with SrTiO_3 . Fortunately, since SrTiO_3 is a very chemically-stable oxide and an industrially ubiquitous material, high-quality single crystals are widely available in market. Also, SrTiO_3 thin films with thicknesses of the second-sound wavelength, namely, 100~500 nm, may be fabricated on various substrate materials. Superconductivity of doped SrTiO_3 ³² would be more interesting if the superconducting phase transition could be externally modulated by coherent temperature waves. We expect many attractive applications of thermal wave utilising SrTiO_3 .

¹ Gurevich, V. L. & Tagantsev, A. K. Second Sound in Ferroelectrics. *Sov. Phys. JETP* **67**, 206–212 (1988).

² Hehlen, B., Pérou, A.-L., Courtens, E. & Vacher, R. Observation of a Doublet in the Quasielastic Central Peak of Quantum-Paraelectric SrTiO_3 . *Phys. Rev. Lett.* **75**, 2416–2419 (1995).

³ Koreeda, A., Takano, R. & Saikan, S. Second Sound in SrTiO_3 . *Physical Review Letters* **99**, 265502(1–4) (2007).

⁴ Martelli, V., Jiménez, J. L., Continentino, M., Baggio-Saitovitch, E. & Behnia, K. Thermal Transport and Phonon Hydrodynamics in Strontium Titanate. *Physical Review Letters* **120**, 1–6 (2018). URL <https://link.aps.org/doi/10.1103/PhysRevLett.120.125901>.

⁵ Huberman, S. *et al.* Observation of second sound in graphite at temperatures above 100 K. *Science (New York, N.Y.)* **3548**, 1–15 (2019). URL <http://arxiv.org/abs/1901.09160> <http://www.ncbi.nlm.nih.gov/pubmed/30872535>. 1901.09160.

⁶ Li, X., Fauqué, B., Zhu, Z. & Behnia, K. Phonon thermal hall effect in strontium titanate. *Phys. Rev. Lett.* **124**, 105901 (2020). URL <https://link.aps.org/doi/10.1103/PhysRevLett.124.105901>.

⁷ Ishito, K. *et al.* Truly chiral phonons in α -hgs (2021). URL <https://arxiv.org/abs/2110.11604>.

⁸ Oishi, E., Fujii, Y. & Koreeda, A. Selective observation of enantiomeric chiral phonons in α -quartz (2022). URL <https://arxiv.org/abs/2210.07526>.

⁹ Ghosh, K., Kusiak, A. & Battaglia, J.-L. Phonon hydrodynamics in crystalline materials. *Journal of Physics: Condensed Matter* **34**, 323001 (2022). 2205.11345.

¹⁰ Ackerman, C. C. & Overton, W. C. Second Sound in Solid Helium-3. *Phys. Rev. Lett.* **22**, 764–766 (1969).

¹¹ Narayananmurti, V. & Dynes, R. C. Observation of Second Sound in Bismuth. *Phys. Rev. Lett.* **28**, 1461–1465 (1972).

¹² Jackson, H. E., Walker, C. T. & McNelly, T. F. Second Sound in NaF. *Phys. Rev. Lett.* **25**, 26–28 (1970).

¹³ Ding, Z. *et al.* Observation of second sound in graphite over 200 K. *Nature Communications* **13**, 1–9 (2022).

¹⁴ Scott, J. F. & Ledbetter, H. Interpretation of elastic anomalies in SrTiO_3 at 37K. *Z. Phys. B* **104**, 635–639 (1997). URL <http://www.springerlink.com/content/u8wuvcl8f5encg1f/>.

¹⁵ Courtens, E., Hehlen, B., Farhi, E. & Tagantsev, A. K. Optical mode crossings and the low temperature anomalies of SrTiO_3 . *Zeitschrift für Physik B Condensed Matter* **104**, 641–642 (1997). URL <http://192.129.24.144/licensed-materials/00257/bibs/7104004/71040641.htm>.

¹⁶ Yamaguchi, M. *et al.* Brillouin-scattering study of the broad doublet in isotopically exchanged SrTiO_3 . *Phys. Rev. B* **65**, 172102 (2002).

¹⁷ Scott, J. F., Chen, A. & Ledbetter, H. The myth of second sound in strontium titanate. *Journal of Physics and Chemistry of Solids* **61**, 185–190 (2000). URL <http://www.sciencedirect.com/science/article/B6TXR-3Y0J888-8/2/445c9018ed83098ed739d5d8d5af2921>.

¹⁸ Koreeda, A., Takano, R. & Saikan, S. Light scattering in a phonon gas. *Physical Review B* **80**, 165104(1–25) (2009). URL <https://link.aps.org/doi/10.1103/PhysRevB.80.165104>.

¹⁹ Scott, J. F. Prospects for ferroelectrics: 2012–2022. *ISRN Materials Science* **2013**, 187313 (2013). URL <https://doi.org/10.1155/2013/187313>.

²⁰ Nakamura, S. & Tsujimi, Y. Broad doublet spectra in the quantum paraelectric state of srtio3. *Ferroelectrics* **485**, 20–26 (2015). URL <https://doi.org/10.1080/00150193.2015.1060086>.

²¹ Koone, C. S., Cohen, M. L., Schooley, J. F., Hosler, W. R. & Pfeiffer, E. R. Superconducting transition temperatures of semiconducting srtio3. *Phys. Rev.* **163**, 380–390 (1967). URL <https://link.aps.org/doi/10.1103/PhysRev.163.380>.

²² Barrett, J. H. Dielectric Constant in Perovskite Type Crystals. *Phys. Rev.* **86**, 118–120 (1952).

²³ Jou, D., Casas-Vázquez, J. & Lebon, G. *Extended Irreversible Thermodynamics* (Springer, Berlin, 2001), 3rd rev edn.

²⁴ Maznev, A. A., Nelson, K. A. & Rogers, J. A. Optical heterodyne detection of laser-induced gratings. *Opt. Lett.* **23**, 1319–1321 (1998). URL <http://ol.osa.org/abstract.cfm?URI=ol-23-16-1319> <http://www.ncbi.nlm.nih.gov/pubmed/18087511>.

²⁵ Tan, M., Tsujimi, Y. & Yagi, T. Broad Doublet Spectra in SrTiO₃. *Journal of the Korean Physical Society* **46**, 97–99 (2005).

²⁶ Koreeda, A., Nagano, T., Ohno, S. & Saikan, S. Quasielastic light scattering in rutile, ZnSe, silicon, and SrTiO₃. *Physical Review B* **73**, 024303 (2006). URL <https://link.aps.org/doi/10.1103/PhysRevB.73.024303>.

²⁷ Koreeda, A., Takano, R., Ushio, A. & Saikan, S. Collective phonon excitation in KTaO₃. *Physical Review B* **82**, 125103(1–7) (2010).

²⁸ Tsujimi, Y. & Itoh, M. Broad Doublet Spectra Observed in Strontium Titanate. *Journal of the Korean Physical Society* **51**, 819–823 (2007).

²⁹ Ashcroft, N. W. & Mermin, N. *Solid State Physics* (Thomson Learning, London, 1976).

³⁰ Buckley, A., Rivera, J. P. & Salje, E. K. H. Twin structures in tetragonal srtio3: The ferroelastic phase transition and the formation of needle domains. *Journal of Applied Physics* **86**, 1653–1656 (1999). URL <https://doi.org/10.1063/1.370942>. <https://doi.org/10.1063/1.370942>.

³¹ Ohno, S., Sonehara, T., Tatsu, E., Koreeda, A. & Saikan, S. Attenuation process of the longitudinal phonon mode in a TeO₂ crystal in the 20-GHz range. *Phys. Rev. B* **95**, 224301 (2017). URL <https://link.aps.org/doi/10.1103/PhysRevB.95.224301>.

³² Gastiasoro, M. N., Ruhman, J. & Fernandes, R. M. Superconductivity in dilute SrTiO₃: A review. *Annals of Physics* **417** (2020), 1912.01509.

³³ Enns, R. H. & Batra, I. P. Stimulated Thermal Scattering in the Second-Sound Regime. *Phys. Rev.* **180**, 227–232 (1969).

³⁴ Batra, I. P., Enns, R. H., ENNS, I. P. B. & H., R. Stimulated thermal scattering of picosecond laser pulses in the second sound limit. *Physics Letters A* **60**, 63–64 (1969). URL <http://www.sciencedirect.com/science/article/B6TVM-46TY11K-1M/2/823ec8e73eea9972a17b06799362b26a>.

³⁵ Müller, K. A. & Burkard, H. SrTiO₃: An intrinsic quantum paraelectric below 4 K. *Phys. Rev. B* **19**, 3593–3602 (1979).

³⁶ Fleury, P. A. & Lyons, K. B. Spectroscopic Observation of Very-Low-Energy Excitations in Glasses. *Phys. Rev. Lett.* **36**, 1188–1191 (1976).

II. METHODS

Stimulated Brillouin scattering by second sound

We used transient grating method for thermal wave (second sound) in dielectric solids. The measurement principle is described in Refs. 33 and 34. As SrTiO₃ is an incipient ferroelectric, the dielectric constant has a rather strong temperature dependence³⁵. Therefore, thermal grating in SrTiO₃ is dominantly formed by coupling of the refractive index or dielectric constant with temperature field, viz., $(\frac{\partial n}{\partial T})_\rho$ or $(\frac{\partial \epsilon}{\partial T})_\rho$, rather than by coupling with density, viz., $(\frac{\partial n}{\partial \rho})_T$ or $(\frac{\partial \epsilon}{\partial \rho})_T$. The incident probe electric field $E(r, t)$ is diffracted as a consequence of the nonlinear polarization due to the temperature fluctuation as

$$P_{\text{NL}}(t) \propto \left(\frac{\partial \epsilon}{\partial T} \right)_\rho \delta T(t) E(t), \quad (3)$$

which leads to a gain factor $G(\omega)$ as³⁴

$$G(\omega) \propto \frac{\alpha_2 E^4}{\rho C_V} \left(\frac{\partial n}{\partial T} \right)_\rho \frac{\omega \Gamma}{(\omega^2 - \omega_0^2)^2 + 4\omega^2 \Gamma^2}, \quad (4)$$

where α_2 is the two-photon absorption coefficient, C_V is the specific heat at constant volume, $\omega_0 = v_{ss} q$ is the eigenfrequency of second sound without damping, v_{ss} is the second-sound velocity, and Γ is the damping rate of the second sound. Here, we considered two-photon absorption²⁶ instead of linear absorption, because SrTiO₃ is transparent for 532 nm radiation of the pump laser employed in our experiments. Accordingly, the corresponding time dependence of the diffracted electric field can be calculated as Fourier transform of Eq. (4) as

$$P_{\text{NL}}(t) \propto \frac{\alpha_2 E^4}{\rho C_V} \left(\frac{\partial n}{\partial T} \right)_\rho \times e^{-\Gamma t} \frac{\sin \sqrt{\omega_0^2 - \Gamma^2} t}{\sqrt{\omega_0^2 - \Gamma^2}}. \quad (5)$$

The temporal behavior of $\delta T(t)$ is alternatively understood as impulsive excitation of a damped harmonic oscillator (DHO).

Writing that $\Omega \equiv \sqrt{\omega_0^2 - \Gamma^2}$ and $\gamma = \sqrt{\Gamma^2 - \omega_0^2} = i\Omega$, the DHO function $f(t)$ can be rewritten as

$$f(t) \propto \begin{cases} e^{-\Gamma t} \frac{\sin \Omega t}{\Omega} & (\omega_0 > \Gamma : \text{underdamped}) \\ e^{-\Gamma t} \frac{\sinh \gamma t}{\gamma} & (\Gamma > \omega_0 : \text{overdamped}) \end{cases} \quad (6)$$

For the underdamping condition $\omega_0 > \Gamma$, $f(t)$ is a damped oscillation with a period of $2\pi/\Omega$ and damping rate of Γ . On the other hand, for the overdamping condition $\Gamma > \omega_0$, $f(t)$ does not oscillate and can be approximated to be double exponential decay as

$$f(t) \approx \frac{e^{-\gamma_1 t} - e^{-\gamma_2 t}}{\gamma_2 - \gamma_1},$$

where $\gamma_1 \approx \frac{\omega_0^2}{2\Gamma} = D_{\text{th}}q^2$ and $\gamma_2 \approx 2\Gamma$, with thermal diffusivity $D_{\text{th}} = \frac{1}{3}\bar{v}_{\text{ph}}^2\tau_R$ and $\Gamma \approx 1/2\tau_R$ (for small value of q). Thus, in the limit of $\Gamma \gg \omega_0$, $f(t)$ leads to an apparent single exponential decay as

$$f(t) \approx \exp(-D_{\text{th}}q^2 t),$$

which is the well-known thermal-diffusion time response.

The squared Fourier amplitudes (intensity spectra) in frequency domain for the underdamped and overdamped cases lead respectively to

$$A_{\text{ud}}^2(\omega) \propto \frac{1}{(\omega_0^2 - \omega^2)^2 + 4\omega^2\Gamma^2}, \quad (7)$$

and

$$A_{\text{od}}^2(\omega) \propto \frac{1}{\omega^2 + D_{\text{th}}q^2}. \quad (8)$$

These are directly compared with the spectra observed in spontaneous Brillouin scattering experiments.

Samples

The samples of SrTiO_3 were synthesised single crystals. We used two samples: Sample A and B. Sample A was purchased at Shinkosha company, Japan, in 1995, which is very slightly amber coloured. Sample B was purchased at Crystal Base, Japan, in 2022, grown by Furuuchi Chemical Corporation, Japan, which was non-coloured and transparent. Both Samples A and B were blocks with dimensions of $10 \times 8 \times 7 \text{ mm}^3$, with surfaces oriented to [001], [110], and [110] in the cubic phase. Our experiments indicated better thermal conductivity of Sample B over Sample A (smaller values of Γ in Sample B).

The transient grating was formed along crystalline [001]_c direction, i.e., the wavevector q was set parallel to [001]_c. Other direction of q provided larger damping constant Γ , probably due to the anisotropy of the thermal conductivity.

Experimental setup

We performed optical heterodyne detection of impulsive stimulated Brillouin/Thermal scattering, which is essentially identical with that presented in Ref.24, although, instead of employing a phase mask, we used a spatial light modulator (SLM: Hamamatsu LCoS-SLM X10468-01) as a zero-order free diffraction grating for both the pump and probe lasers. The grating pitch, i.e., the wavelength of the generated excitation, on the SLM could be quite easily and quickly changed by a personal computer (PC) since an SLM acts as an external display for a PC. We prepared several pictures that had several values of the grating pitches. We used a pulsed

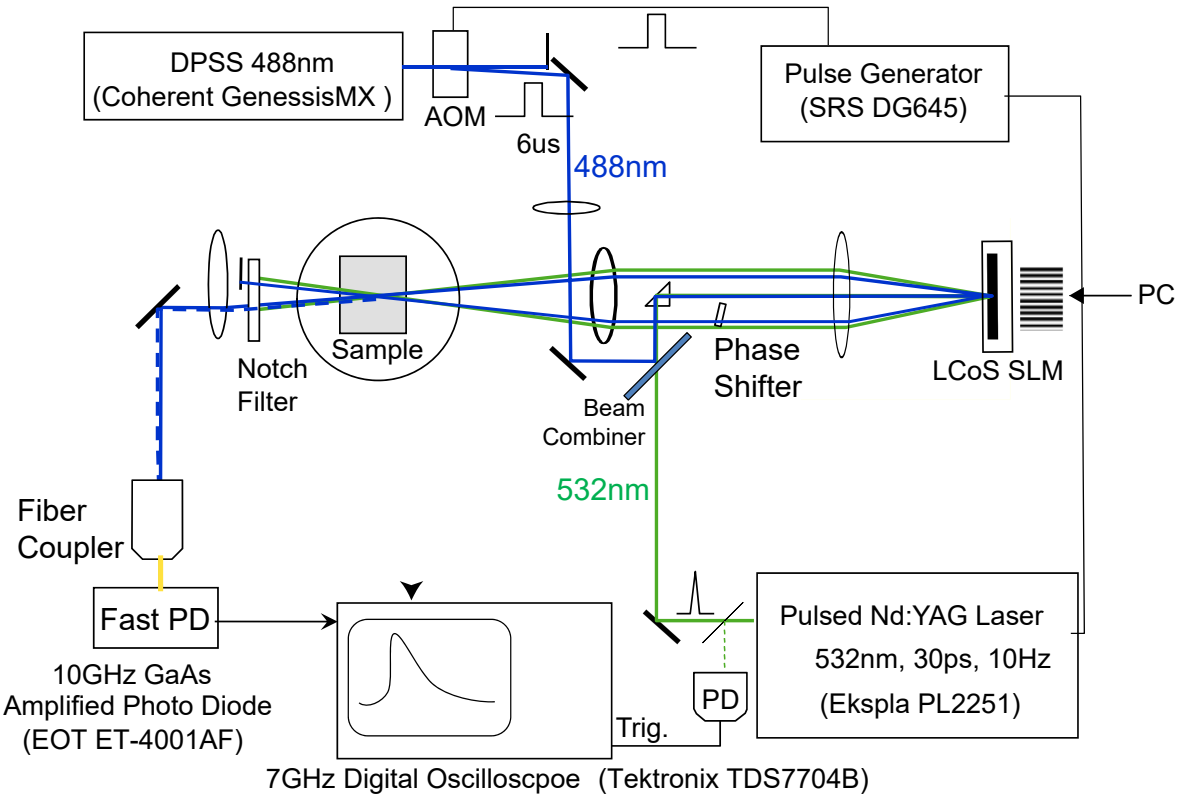
532 nm radiation of the second harmonic from a Nd:yttrium-aluminium-garnet laser with a pulse width of 30 ps (Ekspla PL-1200) as the pump light, and a continuous-wave, single longitudinal mode of 488 nm radiation from a diode-pumped solid state laser (Coherent GenesisMX-SLM) as the probe light. The two beams are collinearly overwrapped and incident on the SLM, and are diffracted back toward the sample. The pairs of the 488 and 532 nm beams were collimated and focused simultaneously in the sample crystal, yielding interference fringes whose pitch exactly coincides for both the pump and probe lights. Since the band gap of SrTiO_3 is ≈ 3.2 eV, the 532 nm light is not linearly absorbed, but two-photon absorption is allowed to produce necessary impulsive heating by non-radiative relaxation of the electronic excited states as previously demonstrated in Refs. 26 and 27. The probe field is diffracted by thermal grating generated by the pump light, perfectly collinearly propagates with the unperturbed probe field (local oscillator), and optically-heterodyne-detected as the beating signal on a fibre-coupled fast photodetector (10GHz GaAs Amplified Photodetector, Electro-optics Technology: ET-4000AF). Thus, the observed signal is proportional to the diffracted electric field, rather than its intensity, and the sign of the signal can be positive and negative. Details are described in Extended Data Fig.1.

ACKNOWLEDGEMENTS

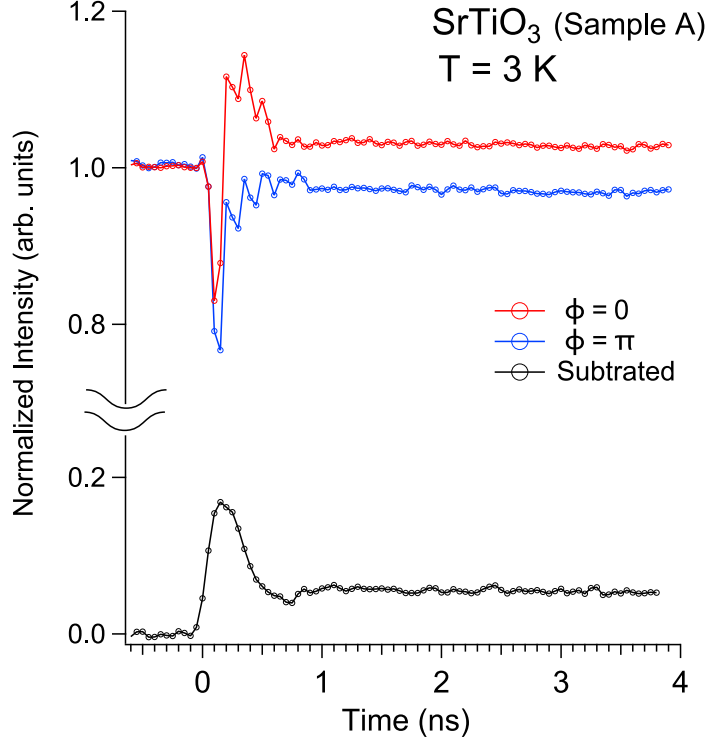
We thank Prof. Toshiro Yagi for his supports and helpful advises at the very early stage of this research project. This work was supported by JSPS KAKENHI Grant Numbers JP17K18765 (A.K. and Y.F.), JP19H05618(A.K.), JP21H01018(A.K. and Y.F.), and JST PRESTO Grant Number JPMJPR10J8 (A.K.).

DECLARATIONS

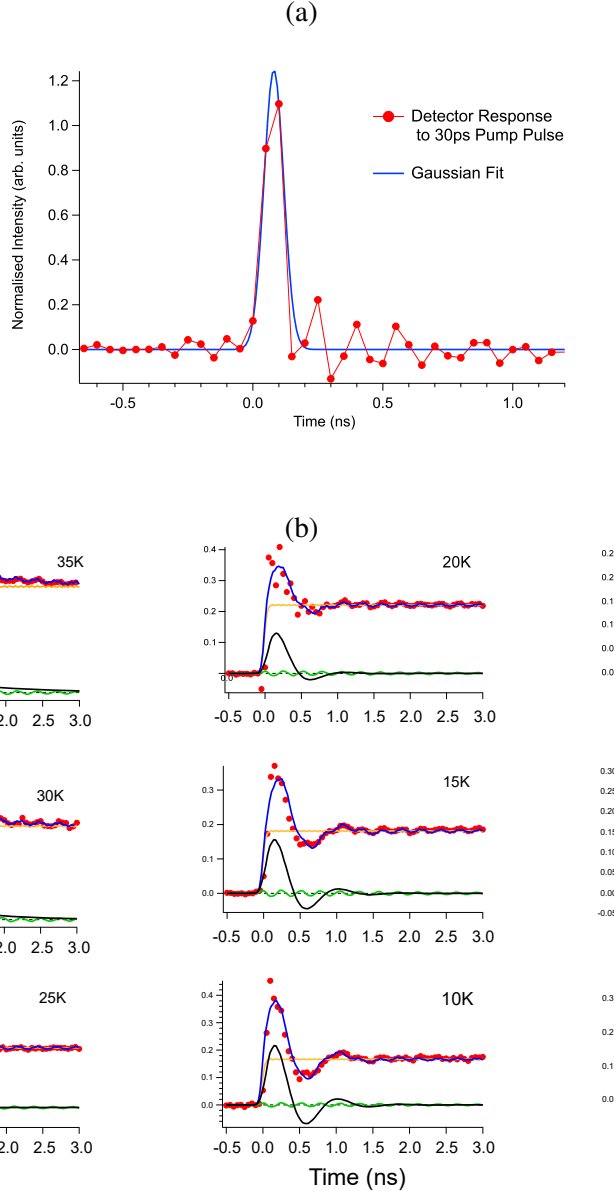
- Conflict of interest/Competing interests
The authors declare no competing interests.
- Availability of data
The datasets generated during and/or analysed during this study are available from the corresponding author upon reasonable request.
- Authors' contributions
A.K. conceived the experiment. H.O., T.O. performed the transient grating measurements, assisted by A.K. and Y.F.. H.O and A.K. analysed and interpreted the results. A.K. wrote the paper. All authors discussed the results.
- Additional information
Extended Data is available for this paper.



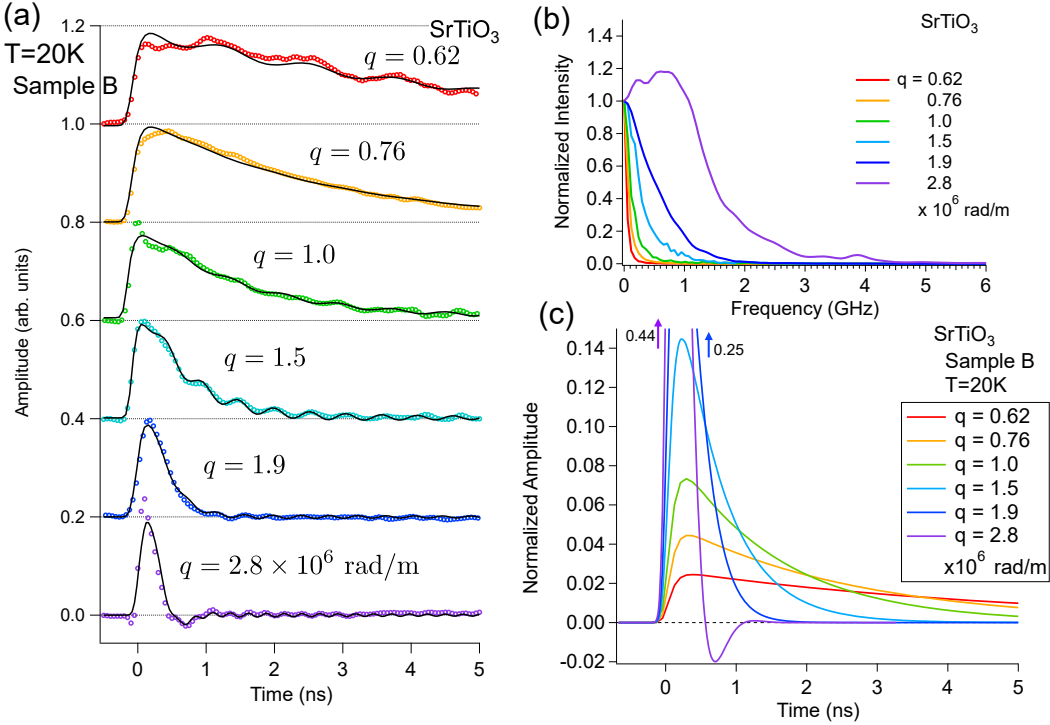
Extended Data Fig. 1. Experimental setup for the generation of coherent thermal wave. AOM: acousto-optic modulator, LCoS SLM: liquid crystal on silicon spatial light modulator, PD: photodiodes, PC: personal computer. We used a pulsed 532 nm radiation of the second harmonic from a Nd:yttrium-aluminum-garnet laser with a pulse width of 30 ps (Ekspla PL-1200) as the pump light, and a continuous-wave, single longitudinal mode of 488 nm radiation from a diode-pumped solid state laser (Coherent GenesisMX-SLM) as the probe light. The probe beam was chopped by an AOM to a 6 μ s pulse to minimize heating of the samples. The two beams are collinearly over-wrapped and incident on an SLM (Hamamatsu LCoS-SLM X10468-01), and are diffracted back toward the sample. The pairs of the 488 and 532 nm beams were collimated and focused simultaneously in the sample crystal, yielding interference fringes whose pitch exactly coincides for both the pump and probe lights. This apparatus is essentially the same with that reported in Ref. 24 with the phasemask replaced by a PC-controlled SLM.



Extended Data Fig. 2. Optically-heterodyne detected signals at phase differences 0 and π , and subtracted signal. The spike and ringing responses commonly present in the raw signals were eliminated by subtraction procedure and only the response of interest can be extracted successfully. The probe field is diffracted by the thermal grating generated by the pump light, perfectly collinearly propagates with the unperturbed probe field (local oscillator), and optically-heterodyne-detected on the photodiode as $I_{\text{det}}^{\pm} \propto |E_{\text{LO}} + E_{\text{sig}}^{\pm}(t)|^2 = I_{\text{LO}}^2 + I_{\text{sig}}^2 \pm 2E_{\text{LO}}E_{\text{sig}}^{\pm}$, where $I_{\text{LO}} = |E_{\text{LO}}|^2$, $I_{\text{LO}} = |E_{\text{sig}}|^2$, and $I_{\text{LO}} \gg I_{\text{sig}}$. The double signs correspond to the relative phases between E_{LO} and $E_{\text{sig}}(t)$, 0 or π . Thus, the observed signal contains a component proportional to the diffracted electric field $E_{\text{sig}}(t)$. By acquiring both signals with relative phases 0 and π and subtraction of them yields $S(t) = I_{\text{det}}^+ - I_{\text{det}}^- \propto 2E_{\text{LO}}[E_{\text{sig}}^+(t) + E_{\text{sig}}^-(t)]$. This procedure is particularly advantageous when E_{sig}^{\pm} carry common noises or residual signals such as a spike due to nonlinear electronic response or detector's ringing response. Since the thermal and acoustic signals change the sign for phase differences between 0 and π while the residual responses not, i.e., $E_{\text{sig}}^{\pm} = \text{Noise} \pm \text{Signal}$, the subtraction procedure eliminates the common residual responses and extracts purely thermal and acoustic responses. All traces presented in the main text were obtained following this procedure.



Extended Data Fig. 3. (a) The photodetector response to a 30 ps laser pulse. We employed a 10 GHz GaAs Amplified Photodetector (Electro-optics Technology: ET-4000AF). The blue curve is a gaussian fit to the initial peak. The effective convolution width was set to 106 ps. Convolution fit with raw detector response, exhibiting a 6 GHz ringing, to the experimental trace was not successful, because the subtracted signal did not virtually contain such ringing responses owing to the elimination of the common noise in the subtraction procedure described in Extended Data Fig. 2. On the other hand, convolution with a gaussian function quite successfully reproduced the experimental signals. So, we decided to employ a gaussian profile obtained by fitting to the initial detector response for convolution fit. (b) Temperature variation of the observed signals and the fitted component functions in the convolution fit. The total fitting function was as follows: $f(t) = \text{heat}(t) + \text{LA}(t) + \text{step}(t)$. Here, $\text{heat}(t) = C_1 \frac{e^{-\Gamma(t-t_0)}}{\Omega} \sin[\Omega(t-t_0)]$, $\text{LA}(t) = C_2 \frac{e^{-\Gamma_B(t-t_0)}}{\Omega_{\text{LA}}} \sin[\Omega_{\text{LA}}(t-t_0) + \phi]$, $\text{step}(t) = \text{const. } (t > 0)$, or $0 (t \leq 0)$, where $\Omega = \sqrt{\omega_0^2 - \Gamma^2}$, $\Omega_{\text{LA}} = \sqrt{\omega_{\text{LA}}^2 - \Gamma_{\text{LA}}^2}$, t_0 , ω_{LA} , Γ_{LA} , and ϕ are a time offset, LA-phonon frequency, LA damping constant, and relative phase of LA mode with respect to second sound (heat function), respectively.



Extended Data Fig. 4. (a) Variation of temporal profiles obtained at $T = 20$ K for various wavenumbers ranging from 6.2×10^5 to $2.8 \times 10^6 \text{ rad/m}$, which correspond to wavelengths ranging from $2.3 \mu\text{m}$ to $10 \mu\text{m}$ (Sample B). At small wavenumbers, the signal appears to be an exponential decay, whereas, at the largest wavenumber, it exhibits an oscillatory behavior. (b) FFT intensity (squared amplitude) spectra of the temporal profiles shown in Fig. 4a, which serve a direct comparison with the spectra of spontaneous light-scattering experiments. For small wavenumbers, the spectra are narrow “central peaks” with a maximum at $\omega/2\pi = 0$. As we increase the wavenumber, the exponential decay becomes faster and the corresponding central-peak spectrum broadens. At the largest wavenumber, the time-domain signal is oscillating with a period of ≈ 1.2 ns, and, accordingly, the spectrum exhibits a resonance peak at ≈ 0.8 GHz. All the time-domain signals were successfully fitted by the damped-harmonic oscillator function, with Γ being fixed to a value of 1.25×10^{10} and $5.56 \times 10^9 \text{ rad/s}$ in Samples A and B, respectively. (c) Normalised signal amplitude of the fitted functions, which demonstrates the transformation from an exponential decay (thermal diffusion) into oscillation (thermal wave) according to the wavenumber of the thermal wave.